Supplementary Information

Partially amorphized $MnMoO_4$ for highly efficient energy storage and hydrogen evolution reaction

Xiaodong Yan,[a] Lihong Tian,[a,b] James Murowchick[b] and Xiaobo Chen[a,*]

a. Department of Chemistry, University of Missouri − Kansas City, Kansas City, Missouri 64110, USA

b. Hubei Collaborative Innovation Center for Advanced Organochemical Materials, Ministry-of-Education Key Laboratory for the Synthesis and Applications of Organic Functional Molecules, Hubei University, Wuhan, Hubei 430062, China

c. Department of Geosciences, University of Missouri – Kansas City, Kansas City, Missouri 64110, USA

* Corresponding author

E-mail address: chenxiaobo@umkc.edu

Experimental Methods

Preparation of hydrogenated $MnMoO_4$

In a typical synthesis, 0.15 mmol of $Mn(NO_3)_2 \cdot 6H_2O$ and 0.02413 mmol of $(NH_4)_6Mo_7O_{24} \cdot 6H_2O$ were dissolved in a solution of 15 mL deionized water in an autoclave. A piece of nickel foam was sonicated in 3 M HCl for 10 min to remove the possible surface oxide layer. After washed with deionized water, the nickel foam was transferred into the above solution and reacted at 160 °C for 6 h (hydrothermal process). After the reaction, the nickel foam was washed with deionized water and dried in air, followed by annealing at 500 °C for 2 h to obtain a $MnMoO_4$ coated Ni foam. The nickel foam was then treated in a high-pressure hydrogen atmosphere at 400 °C for 3 h (hydrogenation), and labeled as H-$MnMoO_4$. The mass loading of the H-$MnMoO_4$ on nickel foam was about 1.2 mg cm^{-2}. In order to investigate the structural evolution of the H-$MnMoO_4$, similar processes were also applied to the powders formed in the hydrothermal process.

Property Characterization

Morphologies of the samples were examined using scanning and transmission electron microscopy (SEM and TEM). The SEM images were taken on a Hatachi 4700 field emission scanning electron microscope (FESEM). The foams were directly mounted on the sample stage for analysis. The TEM study was performed on a FEI Tecnai F20 STEM. The electron accelerating voltage was 200 kV. A small amount of powder sample dispersed in water was dropped onto a thin holey carbon film, and dried overnight before TEM measurement. Structural and chemical properties were studied with X-ray diffraction (XRD) and X-ray photoelectron spectroscopy (XPS). The XRD was performed using a Rigaku Miniflex X-ray diffractometer

using Cu Kα radiation (wavelength = 1.5418 Å). XPS data were collected using a Kratos Axis 165 X-ray photoelectron spectrometer. Spectra were acquired using a photon beam of 1486.6 eV, selected from an Al/Mg dual-anode X-ray source. Fourier transform infrared (FTIR) spectra were recorded on a Thermo-Nicolet iS10 FT-IR spectrometer with an attenuated total reflectance unit.

Electrochemical Characterization

Electrochemical measurements were carried out in a three-electrode system at room temperature. The treated nickel foam, a Pt wire and an Ag/AgCl electrode were used as the working electrode, counter electrode and reference electrode, respectively. 1.0 M KOH solution was used as the electrolyte. Cyclic voltammetry (CV) was performed in the voltage range of 0 − 0.5 V vs. Ag/AgCl at various scan rates from 5 to 80 mV s^{-1} to estimate the capacitive performance of the working electrode. The charge-discharge curves were obtained at a current density of 3 A g^{-1}. The long-term stability test of the samples as electrodes for supercapacitors was conducted at a current density of 7 A g^{-1}. The potential window for the charge-discharge process was set between −0.5 and 0.5 V vs Ag/AgCl. Linear sweep voltammetry was conducted at a scan rate of 5 mV s^{-1} to evaluate the HER performance of the working electrode. Electrochemical impedance spectroscopy (EIS) analysis was performed using a 10 mV amplitude AC signal over a frequency range from 100 kHz to 100 mHz on a Biologic potentiostat/EIS electrochemical workstation. The polarization curve was iR-corrected for an ohmic drop obtained from EIS Nyquist plot. The long-term stability test for HER was performed using constant voltage technique. The reference electrode was calibrated with respect to reversible hydrogen electrode (RHE). The calibration was performed in a high purity hydrogen saturated 1 M KOH electrolyte with a Pt wire as the working electrode. The double layer capacitance (C_{dl}) was measured using a simple cyclic

voltammetry method. The voltage window of cyclic voltammograms was 0.0 – 0.1 V vs RHE. The scan rates were 10, 20, 40, 60 and 80 mV s^{-1}. C_{dl} was estimated by plotting the Δj ($j_a - j_c$) at 0.05 V vs RHE against the scan rate, where the slope was twice as the C_{dl}.

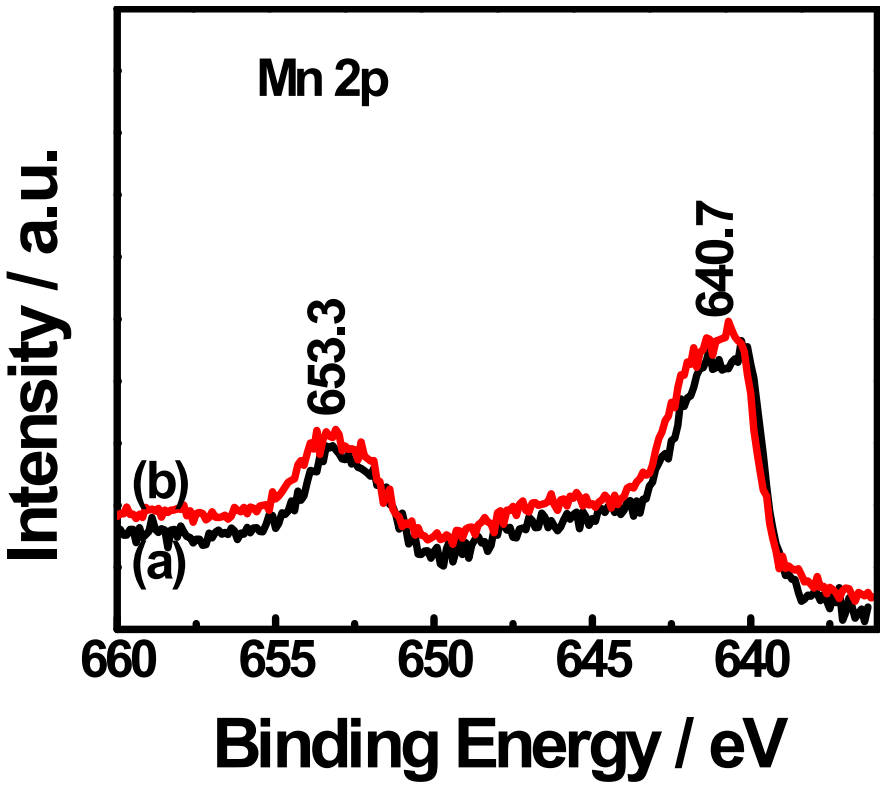

Fig. S1 Mn 2p core-level XPS spectra of (a) $MnMoO_4$ and (b) H-$MnMoO_4$.

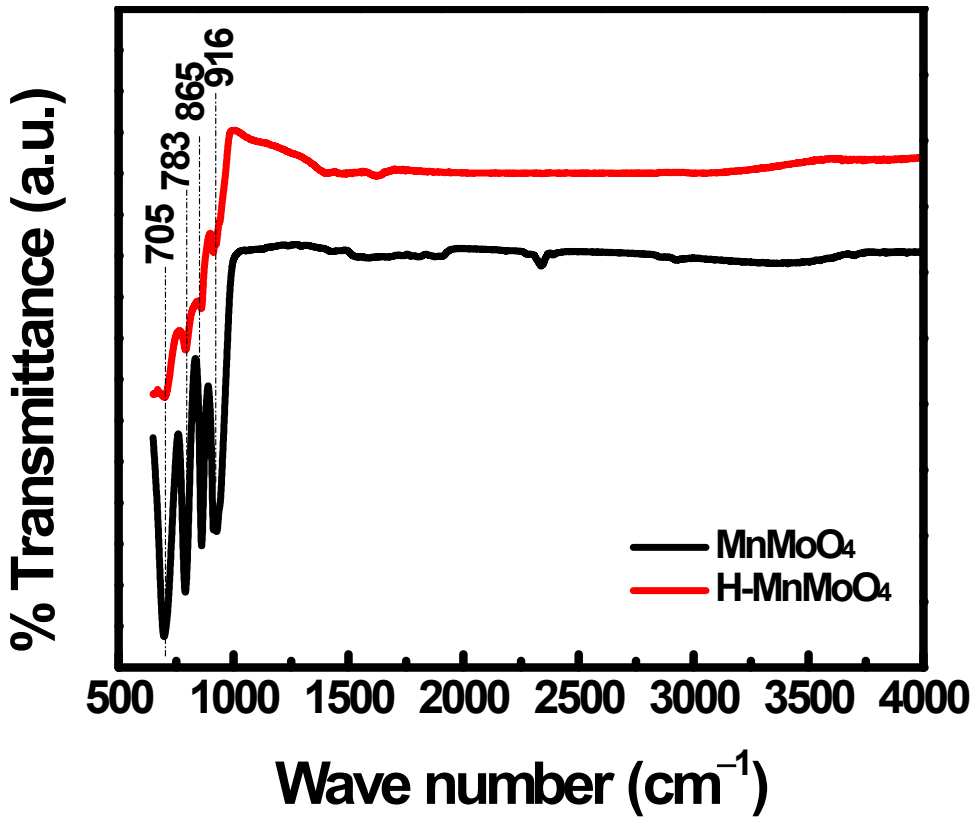

Fig. S2 FTIR spectra of $MnMoO_4$ and H-$MnMoO_4$.

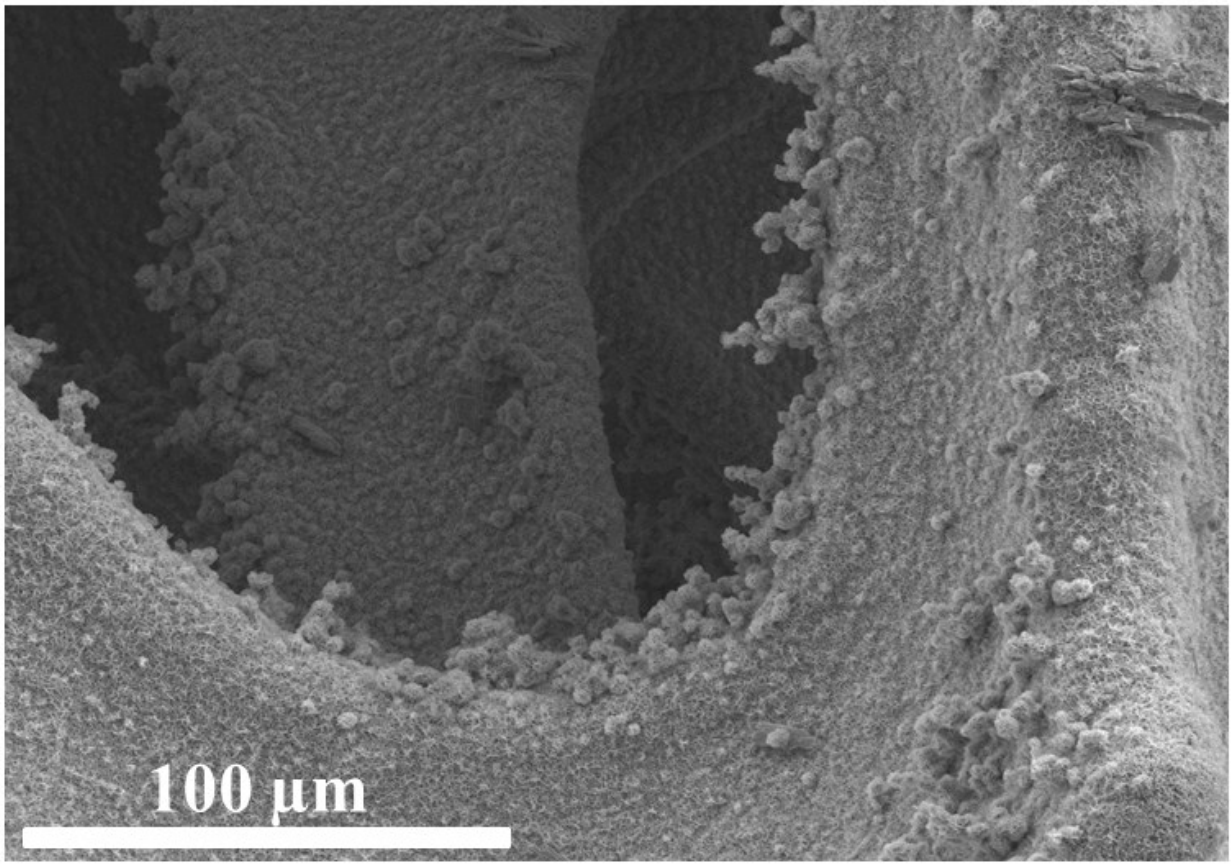

Fig. S3 SEM image of $MnMoO_4$.

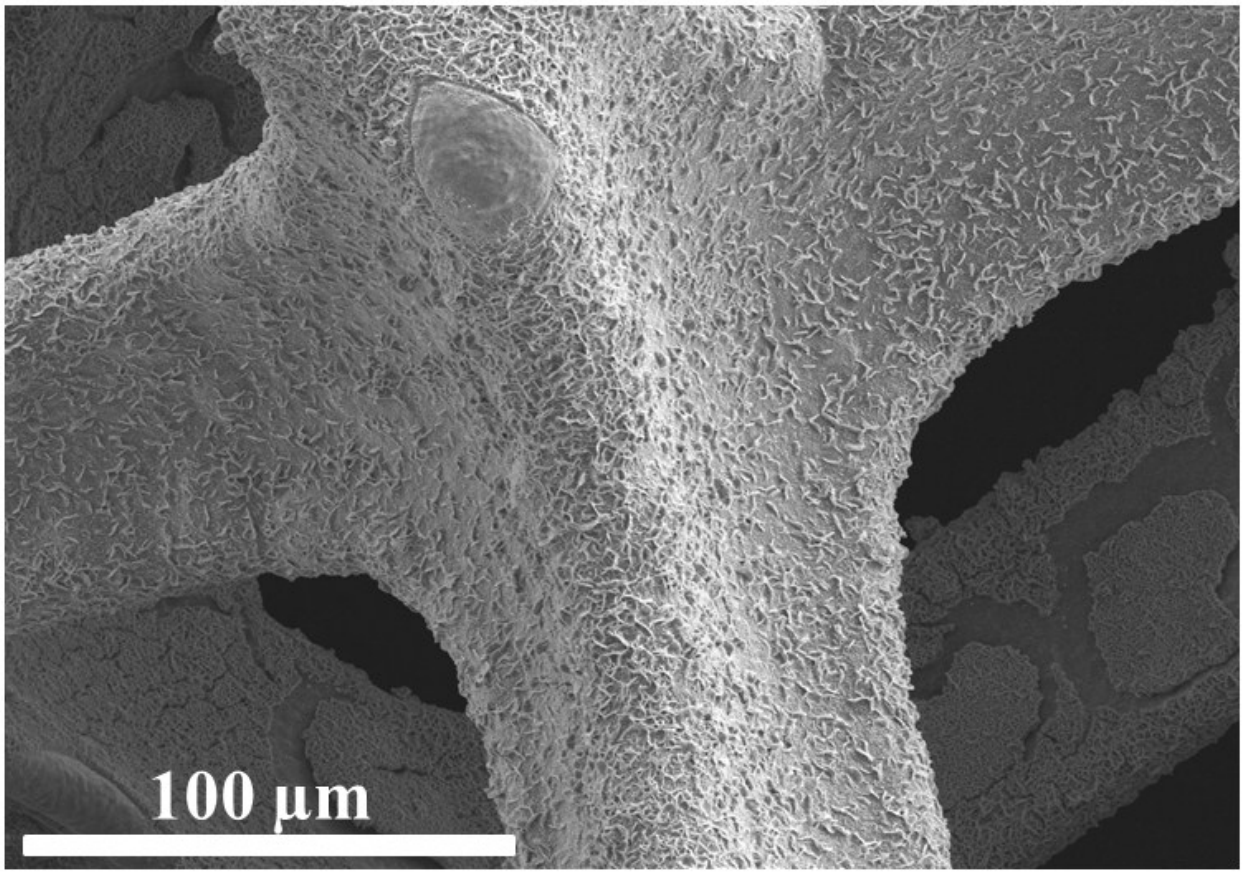

Fig. S4 SEM image of H-$MnMoO_4$.

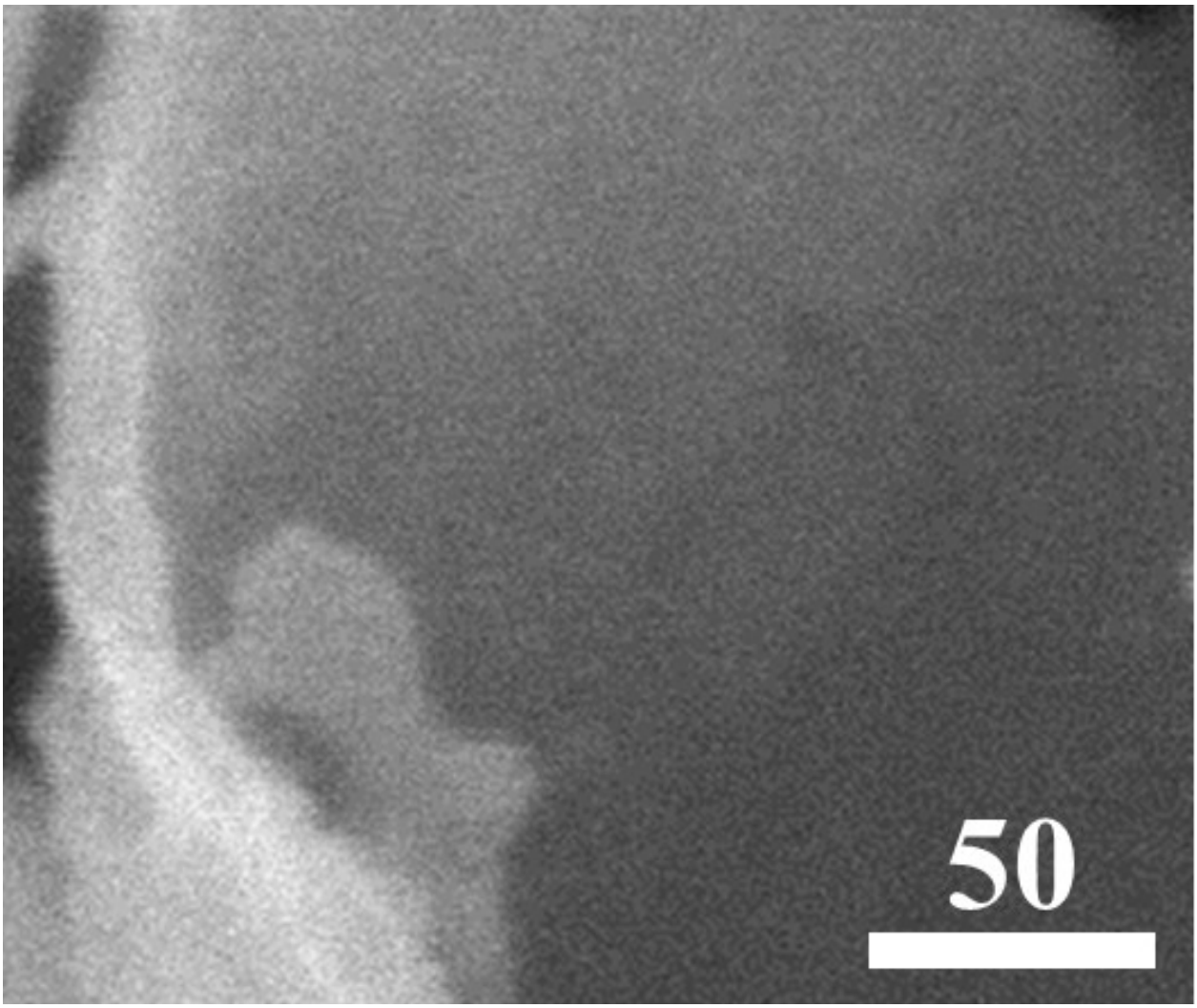

Fig. S5 SEM image of $MnMoO_4$

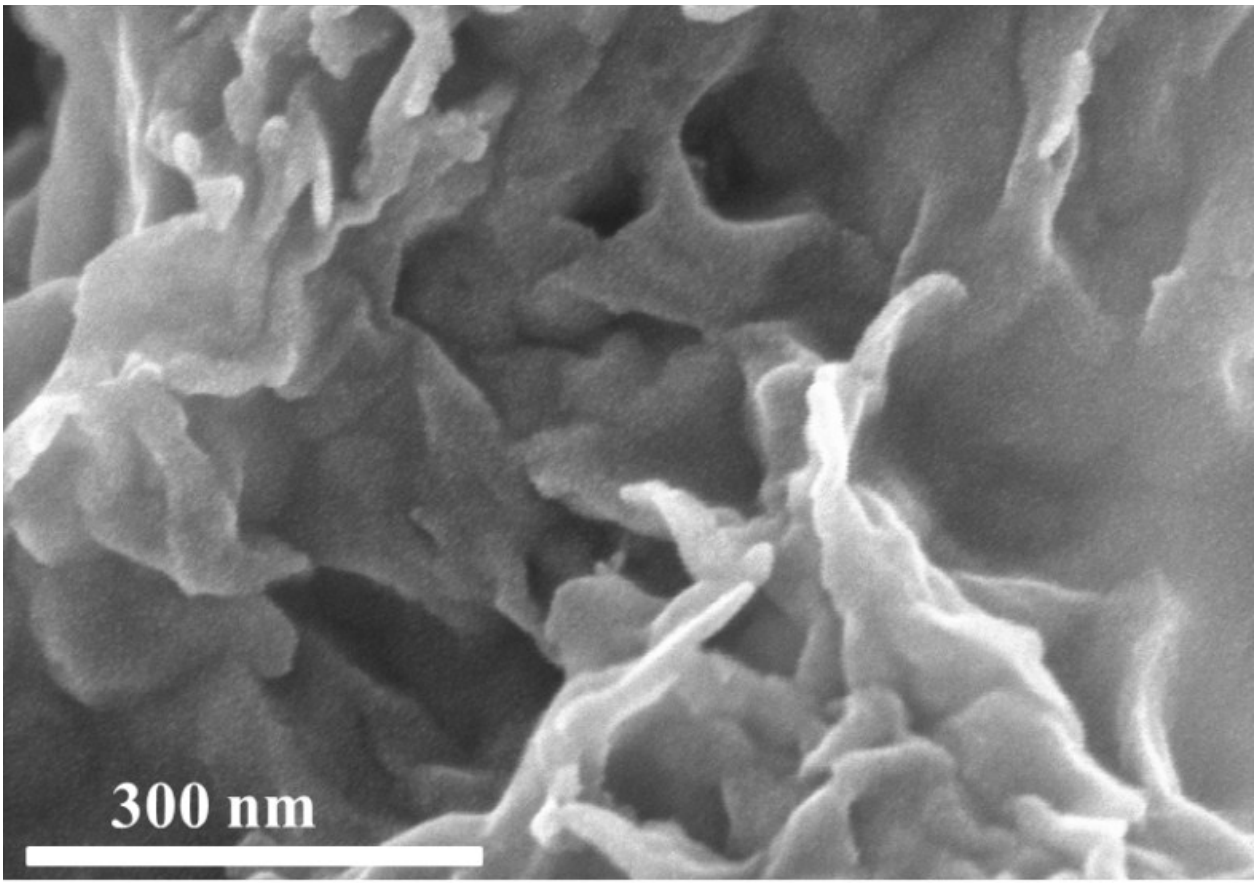

Fig. S6 Magnified SEM image of H-$MnMoO_4$.

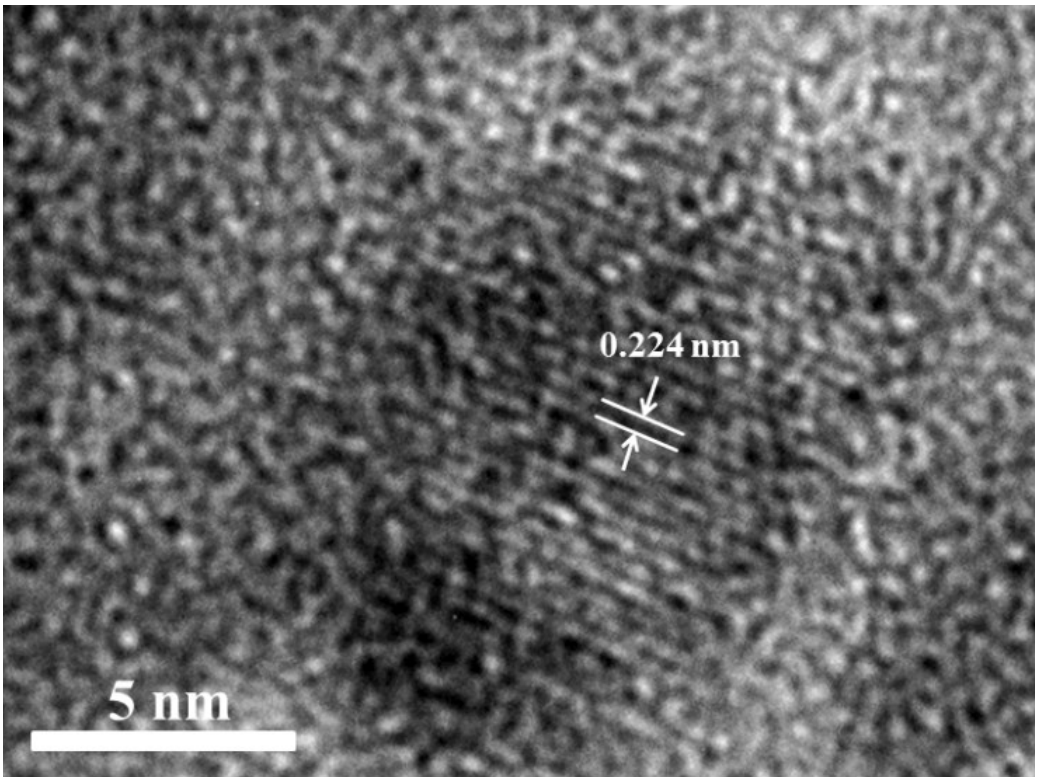

Fig. S7 Magnified TEM image of H-$MnMoO_4$.

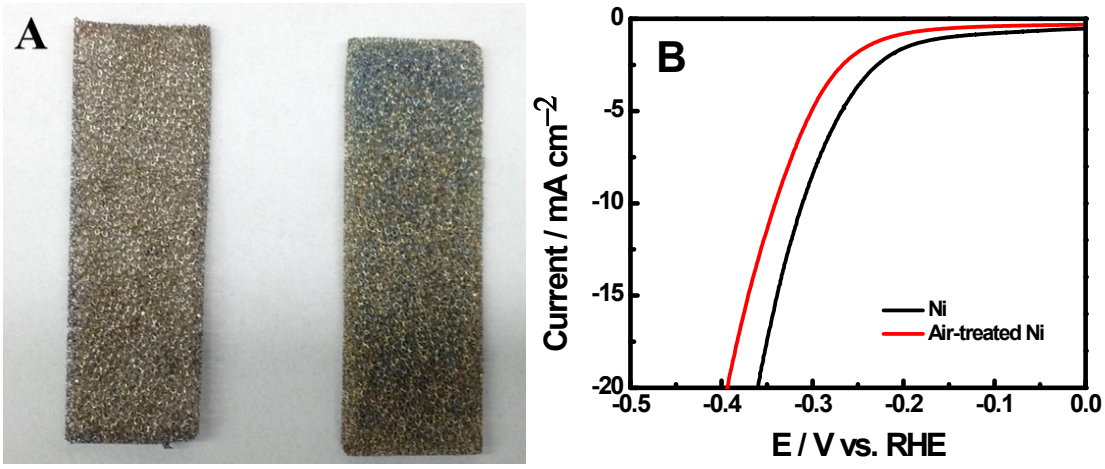

Fig. S8 (A) Digital images of Ni foam before (left) and after (right) heat treatment at 500 °C for 2 h, and (B) Polarization curves of the pristine Ni and air-treated Ni at a scan rate of 5 mV s^{-1}.

In order to verify to which degree the Ni foam was oxidized in air, bare Ni foam was treated in air at 500 °C for 2 h. Very small amount oxide layer was formed on the Ni foam as the color (Fig. S8A) did not change much and polarization curve (Fig. S8B) of the Ni foam after annealing show worse HER performance than before annealing.

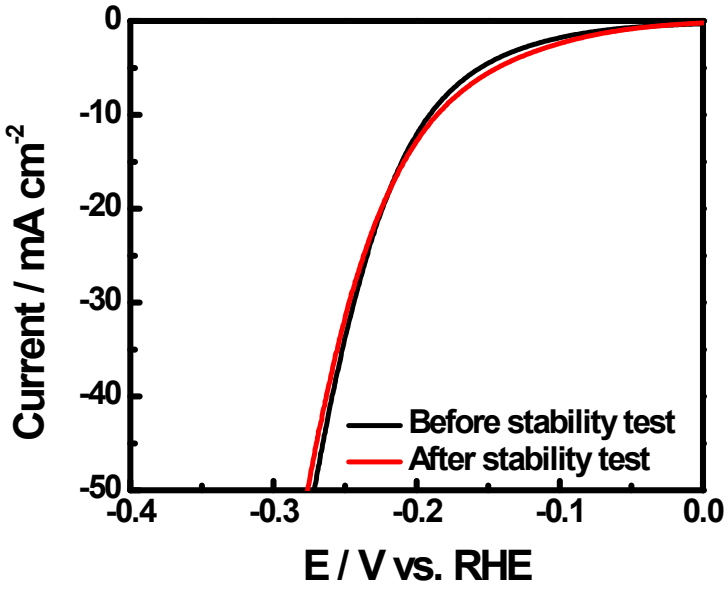

Fig. S9 Polarization curves of the H-$MnMoO_4$ electrode before and after long-term stability test.

Table S1. Comparison of capacitances of different metal molybdate materials.

Sample	Electrolyte	Charge–discharge current	Capacitance ($F\ g^{-1}$)	Ref.
$MnMoO_4$ nanowires	2 M NaOH	1 A g^{-1}	~10	[21]
$MnMoO_4/CoMoO_4$	2 M NaOH	1 A g^{-1}	~187	[21]
α $MnMoO_4$	1 M Na_2SO_4	2 A g^{-1}	234	[22]
α $MnMoO_4$/graphene hybrid	1 M Na_2SO_4	2 A g^{-1}	364	[22]
$MnMoO_4 \cdot 4H_2O$ powder	1 M NaOK	4 mA cm^{-2}	~175	[23]
$MnMoO_4 \cdot 4H_2O$ nanoplates	1 M NaOK	4 mA cm^{-2}	2300	[23]
$MnMoO_4$	1 M KOH	3 A g^{-1}	30	This paper
H- $MnMoO_4$	1 M KOH	3 A g^{-1}	510	This paper

Table S2. Comparison of electrocatalytic activities of different catalysts.

Sample	Electrolyte	η_5 (mV)	Ref.
$Fe_{0.43}Co_{0.57}S_2$	0.5 M H_2SO_4	~170	[36]
$MoSe_2$	0.5 M H_2SO_4	~230	[38]
$MoSe_2$/RGO	0.5 M H_2SO_4	~110	[38]
MoO_2/graphene	0.5 M H_2SO_4	~290	[50]
Co/N-doped carbon	1 M KOH	~175	[S1]
Mn-Ni alloy	0.1 M KOH	~310	[S2]
$MnMoO_4$	1 M KOH	267	This paper
H- $MnMoO_4$	1 M KOH	179	This paper

η_5 reprrsents overpotential at an HER current density of 5 mA cm^{-2}.

[S1] J. Wang, D. Gao, G. Wang, S. Miao, H. Wu, J. Li and X. Bao, J. Mater. Chem. A, 2014,2, 20067−20074.

[S2] M. Ledendecker, G. Clavel, M. Antonietti and M. Shalom, Adv. Funct. Mater. 2015, 25, 393–399.